J. Fluid Mech. (1993), *vol.* 252, *pp.* 147–171

Streaming flow induced by an oscillating cascade of circular cylinders

By B. YAN[1], D. B. INGHAM[1] AND B. R. MORTON[2]

[1] Department of Applied Mathematical Studies, University of Leeds, Leeds, LS2 9JT, UK

[2] Department of Mathematics, Monash University, Clayton 3168, Victoria, Australia

(Received 7 November 1991 and in revised form 28 April 1992)

The fluid flow induced by a cascade of circular cylinders which oscillates harmonically in an unbounded, incompressible, viscous fluid which is otherwise at rest is investigated both numerically and experimentally. Attention in this paper is mainly concentrated on the induced steady streaming flow which occurs when the ratio of the amplitude of the oscillation of the cascade to the size of the cylinder, ϵ, is very small. The leading-order flow is then governed by the steady Navier–Stokes equations. In order to solve these equations numerically we first generate numerically a grid system using the boundary element method and then use a finite-difference scheme on the newly generated rectangular grid system. Numerical results show that for small values of the streaming Reynolds number R_s there are four recirculating flows of equal strength around each circular cylinder of the cascade. At large values of R_s symmetry breaks down and numerical solutions are found for asymmetrical flows. Numerically, a critical value of R_s, R_{s0} say, is identified such that the flow is symmetrical when $R_s < R_{s0}$ and asymmetrical when $R_s > R_{s0}$ and these results are in reasonable agreement with experimental results, which are also presented in this paper.

1. Introduction

It is well known that when a solid body performs small-amplitude, high-frequency, harmonic oscillations in a viscous fluid which is otherwise at rest there is, in addition to the fluctuating component of the flow, a time-independent streaming flow which is induced due to the action of the Reynolds stresses and the Stokes layer which forms on the solid surface. With different combinations of the Reynolds number, $R(= abd/\nu$, where a is the amplitude of the oscillation, d a typical size of the body, b the frequency of oscillation and ν the kinematic viscosity of the fluid), and the parameter which measures the relative amplitude of the oscillation of the motion to the size of the body, $\epsilon(= a/d)$, three different flow regimes have been identified, namely regimes with no boundary layers, one boundary layer and two boundary layers.

When the amplitude of the oscillation is very small and, at the same time, the frequency of the oscillation is very high, then if the streaming Reynolds number, $R_s(= \epsilon R)$, is $O(1)$ the steady streaming flow outside the Stokes layer induced by the oscillating body is governed by the full steady Navier–Stokes equations with the streaming Reynolds number occurring as the parameter. The importance of the streaming Reynolds number was first recognized by Stuart (1963). When $R_s \gg 1$ the induced streaming takes place in a boundary-layer region very close to the body surface but within which the Stokes layer is embedded. For a circular cylinder Stuart (1966) conjectured that these boundary layers ultimately collide and emerge as a jet-like flow along the axis of oscillation. Davidson & Riley (1972) demonstrated both numerically

and experimentally the existence of such streaming boundary-layer flows. Using outer and inner expansion methods Riley (1965, 1967) and Haddon & Riley (1979) (also see Wang 1967) obtained solutions for an oscillating circular cylinder, either in an unbounded fluid or in a finite domain with an outer boundary which is cylindrical in shape, over a wide range of parameters and these results show good agreement with the experimental work of Bertelsen, Svardal & Tjotta (1973) and Bertelsen (1974). With the recently renewed and growing interest in oscillatory viscous flows, Tatsuno & Bearman (1990) have experimentally investigated flow structures over a wide range of parameters and identified eight flow regimes according to different parameters, whilst Stansby & Smith (1991) investigated numerically the viscous forces on a circular cylinder in orbital flow for small values of ϵ and low frequency and their numerical results, for very small values of ϵ, compared well with those they obtained using the outer and inner expansion method.

Historically most of the work on oscillating bodies has been performed for circular cylinders. The axisymmetric geometry of a circular cylinder allowed researchers to simplify the boundary value problem and produce solutions that would be difficult to determine for other geometries. Recently there have been several investigations reported in which the bodies take other shapes and in particular when sharp corners exist and hence singularities occur in the flow field. Irani (1982) and Pattani & Olson (1987, 1988) used the finite element method to investigate the streaming flow initiated by an oscillating square cylinder. Taking advantage of the conformal mapping technique, Kim & Troesch (1989) were able to solve, using a finite-difference method, the streaming flow between two concentric cylinders where the inner square cylinder performs harmonic oscillations and the outer cylindrical cylinder is at rest. Tabakova & Zapryanov (1982) and Zapryanov, Kozhoukharova & Iordanova (1988) investigated the flow fields induced by two circular cylinders, which may be of different radii, which oscillate in a direction which is (i) parallel, or (ii) perpendicular, to the plane of the axes of the cylinders. The effect of the cylinders hydrodynamic interaction on the steady streaming flow has been studied analytically at high values of the frequency of oscillation by the method of matched asymptotic expansion. Experimentally Williamson (1985) has investigated the flows induced by two oscillating cylinders of the same radii in two situations, namely when the flow is induced by two circular cylinders oscillating in a direction which is (i) perpendicular, or (ii) at 45° to the plane of the axes of the cylinders, but the ratio of the amplitude of oscillations to the diameter of the bodies was $O(1)$.

For many-body problems Ingham, Tang & Morton (1990) have examined both numerically and experimentally the steady two-dimensional flow through a cascade of normal flat plates. This work was extended by Ingham & Yan (1989) and Ingham, Yan & Morton (1992) to the situation when the cascade harmonically oscillates but the amplitude of the oscillation is of the same order of magnitude as the size of each plate of the cascade and the frequency of the oscillation was relatively small, i.e. when ϵ, R, $R_b (= R/\epsilon = b^2 d/\nu)$, and R_s are $O(1)$. Further, Ingham & Yan (1992) assumed that the amplitude of the oscillation was very small in comparison with the dimension of the oscillating body, i.e. $\epsilon \ll 1$, and the frequency of oscillation was not too high, or more precisely $R_b = O(1)$, and studied numerically the streaming flow due to the oscillation. They found that the direction of the streaming flow is along the axis of the oscillation and towards the body.

In this paper we numerically investigate the flow induced by a cascade of circular cylinders which performs harmonic oscillations with very small amplitude ($\epsilon \ll 1$) and has a large frequency (i.e. $R_s \geqslant O(1)$) in an unbounded, incompressible fluid which is

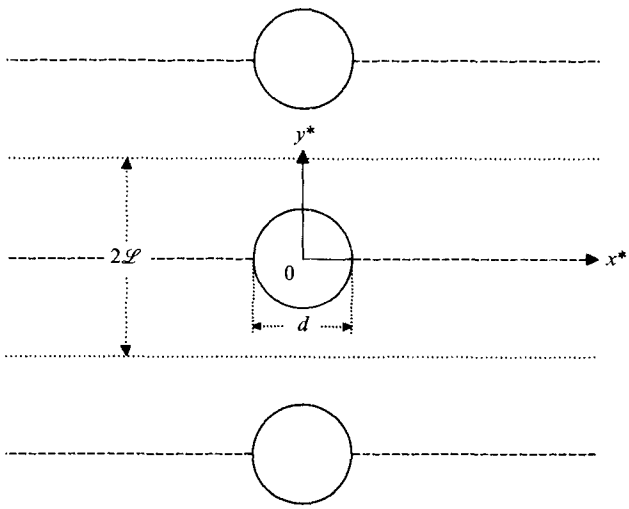

FIGURE 1. The overall cascade geometry.

otherwise at rest. Consistent with the early theories, the leading-order unsteady outer flow is given by the unsteady velocity potential and this flow is determined using a conformal mapping technique which was performed numerically by using grid generation methods (Thompson, Thames & Mastin 1974). Given the tangential velocity next to the body then these inner boundary-layer equations may be solved. The $O(\epsilon)$ outer flow may be determined and this consists of an unsteady component and a steady streaming flow. In this work we use a specialized finite-difference scheme to solve for the steady streaming flow and different kinds of boundary conditions are employed to see their influence on the solution. It is observed that when the streaming Reynolds number is small then the outer steady streaming flow around each cylinder of the cascade is similar to that in the case of one oscillating circular cylinder, whilst different phenomena are observed when this Reynolds number is increased. As the Reynolds number increases then the symmetry of the streaming flow breaks down, i.e. a bifurcation occurs at a critical value of R_s, R_{s0} say, and we have shown, numerically, for $\epsilon \ll 1$ that $8 < R_{s0} < 9$. It is well known that this kind of breakdown of symmetry may be due to the instability of the flow at high values of the Reynolds number (see for example Sobey & Drazin 1986 and Fearn, Mullin & Cliffe 1990).

An experimental investigation has also been performed for the fluid flow induced by an oscillating cascade of circular cylinders with $\epsilon \ll 1$ and the typical size (diameter) of the cylinders being of the same size as the gap width between the cylinders. At small values of the streaming Reynolds number the steady streaming flow is symmetrical whilst at large values of R_s the flow becomes asymmetrical and the experimental results compare well with the present numerical calculations.

2. Governing equations and boundary conditions

Mathematically the fluid flow induced by the harmonic oscillation of an infinite cascade of circular cylinders has been investigated. This cascade consists of an infinite number of circular cylinders of uniform diameter d whose axes occupy the plane $x^* = 0$ at time $t^* = 0$ with each axis at $y^* = 2k\mathscr{L}$, where $k = 0, \pm 1, \pm 2, \ldots$ (see figure 1).

The cascade oscillates harmonically and perpendicular to the plane of the cascade in

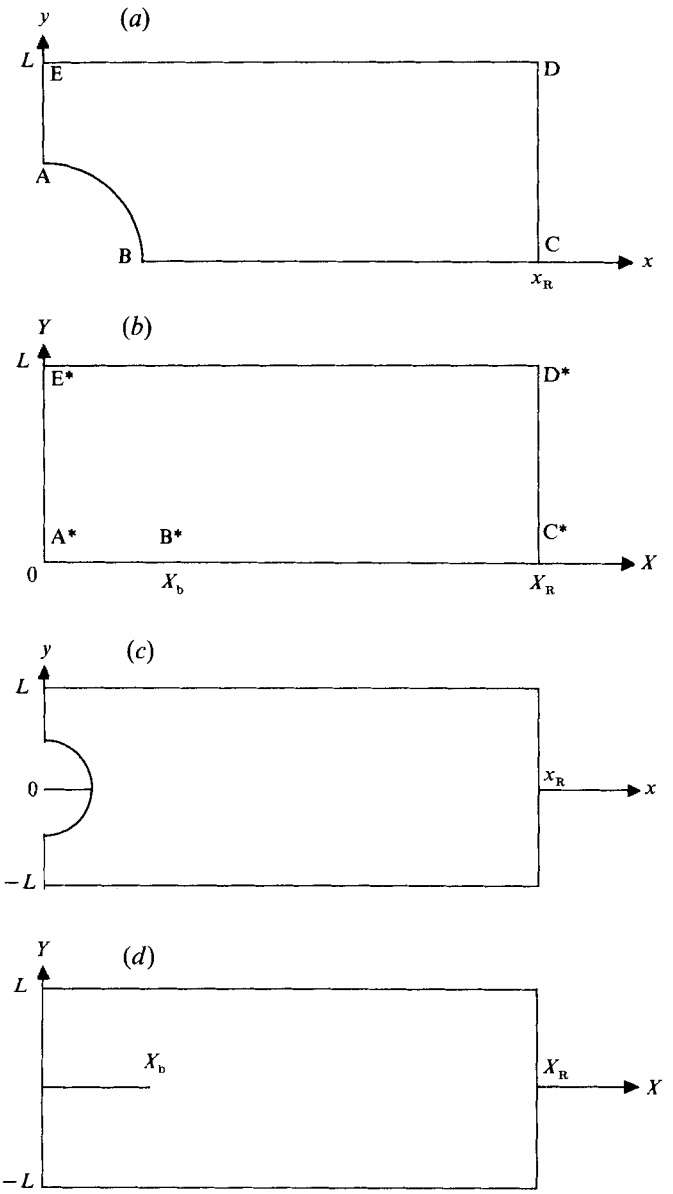

FIGURE 2(*a–d*). For caption see facing page.

an unbounded, incompressible fluid which is otherwise at rest. The displacement of the cascade is in the x^*-direction and is given by

$$s(t^*) = a \sin(bt^*). \tag{2.1}$$

Taking d, b^{-1} and $U(=ab)$ as the length, time and velocity scales and using perturbation 'inner' and 'outer' expansion techniques then the governing non-dimensional equations for the $O(\epsilon)$ outer streaming flow, with the coordinate system fixed in the cascade and in terms of the streamfunction and vorticity, can be written as (see for example Riley 1967)

$$\frac{\partial(\omega, \psi)}{\partial(x, y)} = \frac{1}{R_s} \nabla^2 \omega, \tag{2.2}$$

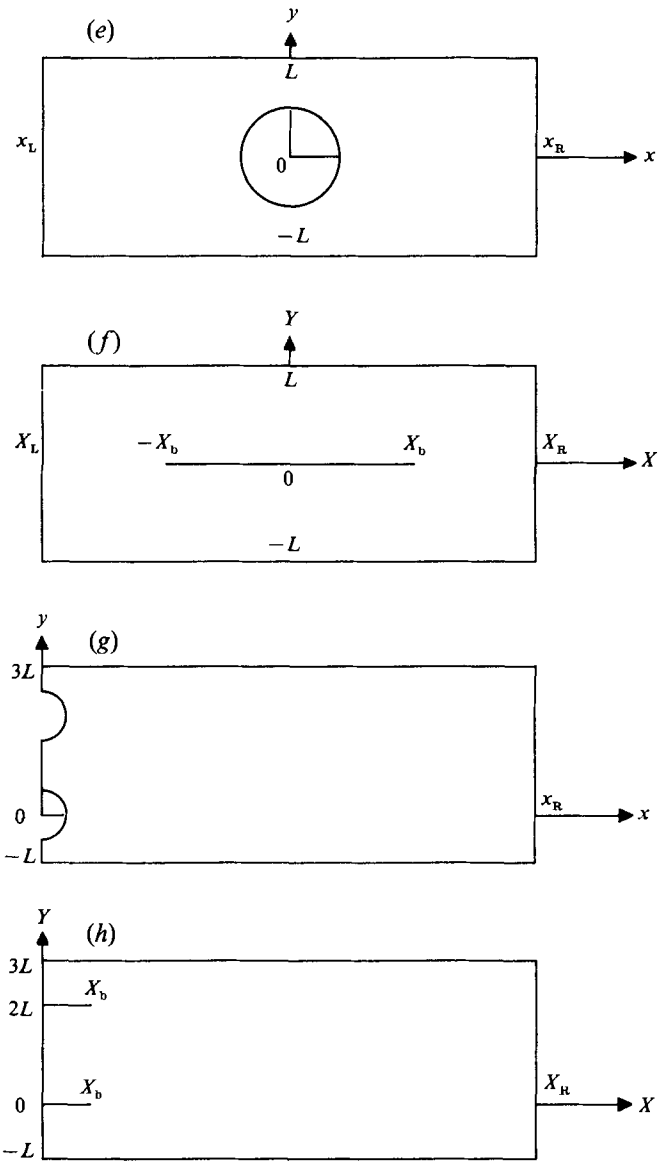

FIGURE 2. Different solution domains. (*a*) DM0, (*b*) transformed DM0, (*c*) DM1 and DM4, (*d*) transformed DM1 and DM4, (*e*) DM2, (*f*) transformed DM2, (*g*) DM3, (*h*) transformed DM3.

$$\nabla^2\psi = -\omega, \tag{2.3}$$

where ψ and ω are the $O(\epsilon)$ steady streamfunction and vorticity, respectively. Equations (2.2) and (2.3) must be solved subject to the following boundary conditions:

$$u_s \equiv \frac{\partial\psi}{\partial n}\bigg|_{x^2+(y\pm 2k\mathscr{L})^2=0.5^2} = -\tfrac{3}{4}u_p\frac{du_p}{ds}, \tag{2.4}$$

$$\psi(x, y: x^2+(y\pm 2k\mathscr{L})^2 = 0.5^2) = 0, \tag{2.5}$$

$$\frac{\partial\psi}{\partial y}\to 0, \quad \omega\to 0, \quad \text{for all} \quad y \quad \text{as} \quad x\to 0, \tag{2.6}$$

where k is an integer, s and n are the variables along and normal to the surface of the

body, u_s is the tangential velocity along the surface of thebody and u_p is the potential tangential velocity along the surface of the body due to the cascade of circular cylinders, see Riley (1967).

Mathematically one would expect the flow to have several symmetries and hence a numerical solution should only be sought in the region $0 \leqslant x < +\infty$, $0 \leqslant y \leqslant L$, see figure 2(*a*). However, experimentally we observe that above a critical value of the Reynolds number the fluid flow breaks these symmetries and hence numerical results have been obtained in solution domains which invoke other symmetries; we will return to these flows in §4.

In order to solve the problem described by (2.2)–(2.6) we first transform the solution domain of the problem in the (x, y)-plane onto a simple domain in a new computational plane and then determine u_p.

3. Grid generation and potential velocity u_p

Owing to the complexity of the physical domain of the problem, we transform it onto a simpler one. In general one can use the following transformation (see Thompson *et al.* 1974):

$$\nabla^2 X = P(X, Y), \tag{3.1}$$

$$\nabla^2 Y = Q(X, Y), \tag{3.2}$$

to transform the domain Ω_p in the (x, y)-plane onto domain Ω_P in the new (X, Y) plane (where the functions P and Q are arbitrary functions which can be used to control the density of the grid lines). The problem is that, in general, transformations (3.1) and (3.2) are not conformal so some substantial changes will be introduced into the governing equations and the potential surface velocity may be difficult to obtain. However, if we take $P = Q = 0$ then (3.1) and (3.2) reduce to

$$\nabla^2 X = 0, \tag{3.3}$$

$$\nabla^2 Y = 0, \tag{3.4}$$

and, subject to some appropriate boundary conditions, (3.3) and (3.4) may become a conformal transformation and the velocity u_p on the surface of the body may be obtained.

Clearly the physical domain of the problem described by (2.2)–(2.6) is infinite in both the x- and y-directions. Because the solution domain is periodic in the y-direction we would expect to have to solve the problem in the domain as shown in figure 2(*a*), as explained earlier. Thus (3.3) and (3.4) have to be solved subject to the following boundary conditions:

$$\frac{\partial X}{\partial n} = 0 \quad \text{when } x^2+y^2 = 0.5^2; \quad 0.5 \leqslant x < +\infty, \quad y = 0; \quad \text{or } 0 \leqslant x < +\infty, \quad y = L, \tag{3.5a}$$

$$\frac{\partial X}{\partial n} = 1 \quad \text{when } x = +\infty, \quad 0 \leqslant y \leqslant L, \tag{3.5b}$$

$$X = 0 \quad \text{when } x = 0, \quad 0.5 \leqslant y \leqslant L, \tag{3.5c}$$

$$Y = 0 \quad \text{when } x^2+y^2 = 0.5^2; \quad 0.5 \leqslant x < +\infty, \quad y = 0, \tag{3.6a}$$

$$Y = y \quad \text{when } x = +\infty, \quad 0 \leqslant y \leqslant L, \tag{3.6b}$$

$$Y = L \quad \text{when } 0 \leqslant x < +\infty, \quad y = L, \tag{3.6c}$$

$$\frac{\partial Y}{\partial n} = 0 \quad \text{when } x = 0, \quad 0.5 \leqslant y \leqslant L, \tag{3.6d}$$

where $L = \mathscr{L}/d$. Equations (3.3)–(3.6) now define a conformal transformation from the (x, y)-plane to the (X, Y)-plane. The governing equations (2.2) and (2.3) become

$$\frac{\partial(\omega, \psi)}{\partial(X, Y)} = \frac{1}{R_s}\nabla^2\omega, \tag{3.7}$$

$$\nabla^2\psi = -\omega/J(X, Y), \tag{3.8}$$

where $J(X, Y)$ is the inverse Jacobian of the transformation.

We now solve (3.3)–(3.6) to obtain X, Y, $\partial X/\partial n$ and $\partial Y/\partial n$ on $\partial\Omega_p$ and u_p on the surface of the body using the boundary element method (BEM). The corresponding inverse problem is solved in the (X, Y) plane to obtain $x(X, Y)$ and $y(X, Y)$ and hence $J(X, Y)(\equiv 1/(J(x, y))$. In this way we can obtain the value of $J(x, y)$ at any given point (X, Y).

It is noted that (3.3) and (3.4) are actually two Laplace equations and only one of them has to be solved, the solution of the other equation then being obtained by using the Cauchy–Riemann equations. Here we solve (3.4) using the linear boundary element method (see for example Manzoor 1984) subject to the boundary conditions (3.6) and at the same time obtain the tangential fluid velocity on the cylinder due to the potential flow induced by the motion of the cascade.

For viable computations we must limit the length of the computational region (say $0 \leqslant x \leqslant x_R$) without introducing significant errors into the results obtained numerically in this region. Therefore the finite value $x = x_R$ at which boundary condition (3.6*b*) (also (2.6)) must be applied should be very large.

Given x_R and the mesh size h, the boundary $\partial\Omega_p$ is divided into N segments: $N = N_1+N_2+N_3+N_4+N_5$, with $N_1 = \text{int}((\frac{1}{4}\pi)/N_3)$, $N_2 = \text{int}((x_R-0.5)/h)$, $N_3 = \text{int}(L/h)$, $N_4 = \text{int}(x_R/h)$ and $N_5 = \text{int}((L-0.5)/h)$ being the number of segments on AB, BC, CD, DE and EA (see figure 2*a*), respectively, then the algebraic system of equations which corresponds to the problem (3.4) and (3.6) may be written as

$$\sum_{j=1}^{N} \mathbb{E}_{ij} Z_j = B(i), \quad i = 1, 2, \ldots, N, \tag{3.9}$$

where

$$B(i) = \sum_{j=1}^{N} \mathbb{G}_{ij} \bar{Z}_j, \quad \{\bar{Z}_j\}_1^N = \{Y_1, \ldots, Y_{N-N_5}, Y'_{N-N_5+1}, \ldots, Y'_N\},$$

$\{Z_j\}_1^N = \{Y'_j\}_1^{N-N_5} \cup \{Y_j\}_{N-N_5+1}^N$ and all of the elements of $\mathbb{E}$ and $\mathbb{G}$ are known. The system of equations (3.9) can then be solved by the standard Gaussian-elimination method. The values of X_j and X'_j on $\partial\Omega_P$ can now be calculated by using the Cauchy–Riemann equations

$$\frac{\partial X}{\partial y} = \frac{\partial Y}{\partial x}, \quad \frac{\partial X}{\partial x} = -\frac{\partial Y}{\partial y}. \tag{3.10}$$

The solution Y represents the potential flow due to the cascade and therefore u_p can be obtained from

$$u_p = -\partial Y/\partial n. \tag{3.11}$$

The problem now is to find an appropriate value of x_R such that the BEM gives a solution of (3.4) and (3.6) to a high degree of accuracy. In all the calculations presented in this paper it is found that $x_R = 15$ is sufficiently large, since any further increase in this value only results in changes in the value of u_p of less than 1%.

On knowing all the values of X, X', Y and Y' we can now use them to calculate the corresponding values of x, x', y and y' on $\partial\Omega_P$ in the (X, Y)-plane. Actually $x = x(X, Y)$ and $y = y(X, Y)$ in the domain as shown in figure 2(*b*) satisfy the Laplace equations

$$\nabla^2 x = 0, \tag{3.12}$$

$$\nabla^2 y = 0. \tag{3.13}$$

Knowing the values of x, x', y and y' on $\partial\Omega_P$, the solutions of (3.12) and (3.13) may be obtained by using the Green's integral formulae and hence $J(x, y) = 1/J(X, Y)$ can be obtained at any point (X, Y) in the (X, Y)-plane that is required when solving (3.7) and (3.8).

4. Numerical procedure

4.1. *Boundary conditions*

Apart from the boundary conditions (2.4) and (2.5) we need to determine the vorticity on the surface of the body, i.e. for $|X| \leqslant X_b$, $Y = 0+$ in the (X, Y)-plane, see figure 2(*b*). Using the Taylor expansion method at a boundary point B then, for the first internal point from B, say I, it can be shown that

$$\omega_B = \frac{6\psi_B - 6\psi_I - 6h_Y u_s/(\partial Y/\partial n)_B - h_Y^2 J(x_B, y_B)\omega_I}{h_Y^2[h_Y(\partial J(x, y)/\partial Y)_B + 2J(x_B, y_B)]}. \tag{4.1a}$$

It should be noted that (4.1*a*) cannot be used at the points $(x_B, y_B) = (0.5, 0)$ and $(-0.5, 0)$ owing to the singularity of the transformation (3.4)–(3.6). However, bearing in mind that both the streamfunction and the vorticity are not singular at these points, then the values of the vorticity at these points may be obtained using an (r, θ) coordinate system. Thus at $(r_B, \theta_B) = (0.5, 0)$ and $(0.5, \pi)$, which correspond to $(x_B, y_B) = (0.5, 0)$ and $(-0.5, 0)$ in the (x, y)-plane, respectively, the vorticity is given by

$$\omega_B = \frac{6\psi_B - 6\psi_I + 2\delta r(3 - 3\delta r + 4\delta r^2)\, u_s + \dfrac{\delta r^2 \omega_{I1}}{k(k+1)} - \dfrac{\delta r^2(1+k)\,\omega_I}{k}}{\delta r^2\left(3 + 2\delta r - \dfrac{2+k}{1+k}\right)}, \tag{4.1b}$$

where I1 is the second internal point from the boundary point B, $(r_B, \theta_B) = (0.5, 0)$ or $(0.5, \pi)$), $\delta r = r_I - r_B$ and $k = (r_{I1} - r_B)/\delta r$.

Owing to the symmetry of the problem, in addition to the boundary conditions (2.4)–(2.6) and (4.1) the following symmetrical boundary conditions are applied:

DM0: Mathematically we can enforce a set of symmetrical boundary conditions about both $x = 0$ and $y = 0$ and then take the solution domain as shown in figure 2(*a*) due to the symmetry of the physical domain, i.e.

$$\psi = \omega = 0 \quad \begin{cases} \text{when } x \geqslant 0.5, & y = 0 \\ \text{and when } 0 \leqslant x \leqslant x_R, & y = L, \end{cases} \tag{4.2a}$$

$$\psi = 0 \quad \text{when } x = 0, \quad 0.5 \leqslant y \leqslant L. \tag{4.2b}$$

However, the physical solution of the problem may not be symmetrical for large values of R_s. Indeed, as will be shown in our experimental results (see §6), the streaming flow is symmetrical when the streaming Reynolds number R_s is small and asymmetrical when R_s is large. This breakdown in symmetry of the flow is similar to that obtained

in the two-dimensional sudden-expansion channel flow which becomes asymmetrical at about $R = 40$, see Fearn *et al.* (1990). In order to predict the experimentally observed solutions then the boundary condition (4.2) must be relaxed. Therefore some different asymmetrical boundary conditions for the possible solution remains as shown in figure 2 have been considered, namely:

DM1: We relax the symmetrical boundary conditions about $y = 0$ and solve the problem in the solution domain DM1 (see figure 2*c*) subject to the following boundary conditions:

$$\psi|_{y=L} = \psi|_{y=-L} \quad \text{when } 0 \leqslant x \leqslant x_R, \tag{4.3a}$$

$$\omega|_{y=L} = \omega|_{y=-L} \quad \text{when } 0 \leqslant x \leqslant x_R, \tag{4.3b}$$

$$\left.\frac{\partial\psi}{\partial x}\right|_{(0,y)} = -\left.\frac{\partial\psi}{\partial x}\right|_{(0,-y)} \quad \text{when } 0.5 \leqslant y \leqslant L, \tag{4.3c}$$

$$\left.\frac{\partial\omega}{\partial x}\right|_{(0,y)} = -\left.\frac{\partial\omega}{\partial x}\right|_{(0,-y)} \quad \text{when } 0.5 \leqslant y \leqslant L. \tag{4.3d}$$

The vorticity on $0 \leqslant X < X_b$ and $Y = 0+$ is given by (4.1*a*) whilst on $0 \leqslant X < X_b$ and $Y = 0-$, see figure 2(*d*), the vorticity is given by

$$\omega_B = \frac{6\psi_B - 6\psi_I + 6h_Y u_s \Big/ \left(\dfrac{\partial Y}{\partial n}\right)_B - h_Y^2 J(x_B, y_B)\omega_I}{h_Y^2\left[h_Y\left(\dfrac{\partial J(x,y)}{\partial Y}\right)_B + 2J(x_B, y_B)\right]}. \tag{4.3e}$$

DM2: We now relax the symmetry conditions about $x = 0$ and $y = 0$ and therefore we have to solve the governing equations (2.2) and (2.3) in the solution domain as shown in figure 2(*e*). Hence the boundary conditions (4.3*a*) and (4.3*b*) must be supplemented by the boundary conditions

$$\psi|_{y=L} = \psi|_{y=-L} \quad \text{when } x_L \leqslant x \leqslant x_R, \tag{4.4a}$$

$$\omega|_{y=L} = \omega|_{y=-L} \quad \text{when } x_L \leqslant x \leqslant x_R. \tag{4.4b}$$

The boundary condition for the vorticity on the surface of the body, i.e. on $-X_b < X < X_b$ and $Y = 0+$ in the (X, Y) plane, see figure 2(*f*), is given by (4.1*a*), whilst on $-X_b < X < X_b$ and $Y = 0-$ the vorticity is given by (4.3*e*).

DM3: In this case we assume, again, that the flow is periodic in the y-direction but with a period of symmetry four times that of the fundamental solution. Hence we solve the governing equations (2.2) and (2.3) in the region described by figure 2(*g*). The boundary conditions (4.2) then have to be supplemented by the following boundary conditions:

$$\psi|_{y=3L} = \psi|_{y=-L}, \quad \text{when } 0 \leqslant x \leqslant x_R, \tag{4.5a}$$

$$\omega|_{y=3L} = \omega|_{y=-L}, \quad \text{when } 0 \leqslant x \leqslant x_R, \tag{4.5b}$$

$$\left.\frac{\partial\psi}{\partial x}\right|_{(0,y)} = -\left.\frac{\partial\psi}{\partial x}\right|_{(0,2L-y)} \quad \text{when } -L \leqslant y \leqslant -0.5 \text{ or } 0.5 \leqslant y \leqslant L, \tag{4.5c}$$

$$\left.\frac{\partial\omega}{\partial x}\right|_{(0,y)} = -\left.\frac{\partial\omega}{\partial x}\right|_{(0,2L-y)} \quad \text{when } -L \leqslant y \leqslant -0.5 \text{ or } 0.5 \leqslant y \leqslant L. \tag{4.5d}$$

The boundary conditions for the vorticity on the surface of the bodies, i.e. on $0 \leqslant X < X_b$ and $Y = 0+$, $Y = 2L+$ are given by (4.1*a*) whilst on $0 \leqslant X < X_b$ and $Y = 0-$, $y = 2L-$, see figure 2(*h*), the vorticity is given by (4.3*e*).

DM4: In DM1 we have used antisymmetrical boundary conditions about $x = 0$ and periodic boundary conditions on $y = -L$ and $y = L$. In this section we apply the following boundary conditions to the solution domain DM1, see figure 2(*c*):

$$\psi|_{y=L} = \psi|_{y=-L} \quad \text{when } 0 \leqslant x \leqslant x_R, \tag{4.6a}$$

$$\omega|_{y=L} = \omega|_{y=-L} \quad \text{when } 0 \leqslant x \leqslant x_R, \tag{4.6b}$$

$$\psi|_{(x,y)} = -\psi|_{(-x,y)} \quad \text{when } -L \leqslant y \leqslant -0.5, \quad 0.5 \leqslant y \leqslant L, \tag{4.6c}$$

$$\omega|_{(x,y)} = -\omega|_{(-x,y)} \quad \text{when } -L \leqslant y \leqslant -0.5, \quad 0.5 \leqslant y \leqslant L, \tag{4.6d}$$

and the boundary conditions for the vorticity on the surface of the cylinder are those used in DM1 and are given by (4.1*a*) and (4.3*e*).

Other less severe symmetries can be considered but this will increase the size of the computational domain and hence the computational time. Therefore such flows have not been investigated.

If the solution at a given value of R_s is symmetrical about $x = 0$ then the solution obtained by solving in domain DM1 will be the same as that obtained when using domain DM4.

4.2. *Numerical procedure*

The numerical procedure used in this paper is as follows:

(*a*) Take $x_R = 15$ and obtain u_s (see §3);

(*b*) solve (3.3) and (3.4) subject to the boundary conditions (3.5)–(3.6) on $\partial\Omega_p$ and then solve the inverse problem (3.12) and (3.13) on $\partial\Omega_P$ by using the BEM (see §3);

(*c*) use Green's integral formula to calculate $x = x(X, Y)$ and $y = y(X, Y)$ and then obtain $J(x, y)$ in the (X, Y)-plane;

(*d*) solve (3.7) and (3.8) according to the numerical scheme as described below.

Following Ingham & Yan (1989), in order to reduce the number of grid points in the X-direction and at the same time maintaining the number of grid points near $X = 0$ (i.e. near the cylinder) we introduce the following transformation in the X-direction:

$$\xi = \begin{cases} X & \text{when } |X| \leqslant X_b \\ X_b + \ln[1 + A_d(X - X_b)] & \text{when } X > X_b \\ -X_b - \ln[1 - A_d(X + X_b)] & \text{when } X < -X_b, \end{cases} \tag{4.7}$$

where X_b is the X-component of the image of B (see figure 2) in the (X, Y) plane and A_d is a constant such that the mesh sizes in the X-direction on both sides of $X = X_b$ are the same for a given mesh size in the ξ-direction of the (ξ, Y) plane.

The governing equations (3.7) and (3.8) now become:

when $|\xi| > X_b$

$$E(\xi)\frac{\partial(\omega, \psi)}{\partial(\xi, Y)} \pm \frac{E^2(\xi)}{R_s}\frac{\partial\omega}{\partial\xi} = \frac{1}{R_s}\left[E^2(\xi)\frac{\partial^2\omega}{\partial\xi^2} + \frac{\partial^2\omega}{\partial Y^2}\right], \tag{4.8}$$

$$E^2(\xi)\left[\frac{\partial^2\psi}{\partial\xi^2} \mp \frac{\partial\psi}{\partial\xi}\right] + \frac{\partial^2\psi}{\partial Y^2} = -\frac{\omega}{J(X(\xi), Y)}; \tag{4.9}$$

when $|\xi| \leqslant X_b$

$$\frac{\partial(\omega, \psi)}{\partial(\xi, Y)} = \frac{1}{R_s}\left[\frac{\partial^2\omega}{\partial\xi^2} + \frac{\partial^2\omega}{\partial Y^2}\right], \tag{4.10}$$

$$\frac{\partial^2\psi}{\partial\xi^2} + \frac{\partial^2\psi}{\partial Y^2} = -\frac{\omega}{J(X(\xi), Y)}, \tag{4.11}$$

where $X(\xi)$ is the inverse function of (4.7) and

$$E(\xi) = A_d \exp(-(\xi - X_b)) \quad \text{when } \xi > X_b, \tag{4.12}$$

$$E(\xi) = A_d \exp(\xi + X_b) \quad \text{when } \xi < -X_b, \tag{4.13}$$

and the upper sign in (4.8) and (4.9) occurs when $\xi > X_b$ whilst the lower sign occurs when $\xi < -X_b$.

A modified central-difference scheme (see Dennis & Hudson 1978) which is similar to that used by Ingham *et al.* (1992) for the unsteady cascade flow is used to discretize (4.8) and (4.10). Taking h_ξ and h_Y to be the mesh sizes in the ξ- and Y-directions, respectively, and using the subscripts 0, 1, 2, 3 and 4 to denote typical grid points (ih_ξ, jh_Y), $((i+1)h_\xi, jh_Y)$, $(ih_\xi, (j+1)h_Y)$, $((i-1)h_\xi, jh_Y)$, $(ih_\xi, (j-1)h_Y)$, respectively, then the finite-difference representation of (4.8)–(4.11) can be written as

$$c_1\omega_1 + c_2\omega_2 + c_3\omega_3 + c_4\omega_4 - c_0\omega_0 = 0, \tag{4.14}$$

$$b_1\psi_1 + b_2\psi_2 + b_3\psi_3 + b_4\psi_4 - b_0\psi_0 + h_\xi^2 h_Y^2 \omega_0 / J(X(\xi_0), Y_0) = 0, \tag{4.15}$$

where

$$c_1 = \begin{cases} E_0 h_Y^2 \left\{1 \mp \tfrac{1}{2}h_\xi \left[E_0 \pm R_s\left(\dfrac{\partial\psi}{\partial Y}\right)_0\right] + \tfrac{1}{8}h_\xi^2 \left[E_0 \pm R_s\left(\dfrac{\partial\psi}{\partial Y}\right)_0\right]^2\right\}, & |\xi| > X_b \\ h_Y^2 \left\{1 - \tfrac{1}{2}h_\xi R_s\left(\dfrac{\partial\psi}{\partial Y}\right)_0 + \tfrac{1}{8}h_\xi^2 R_s^2\left(\dfrac{\partial\psi}{\partial Y}\right)_0^2\right\}, & |\xi| \leqslant X_b, \end{cases}$$

$$c_2 = \begin{cases} h_\xi^2 \left\{1 + \tfrac{1}{2}h_Y R_s E_0\left(\dfrac{\partial\psi}{\partial\xi}\right)_0 + \tfrac{1}{8}h_Y^2 R_s^2 E_0^2\left(\dfrac{\partial\psi}{\partial\xi}\right)_0^2\right\}, & |\xi| > X_b \\ h_\xi^2 \left\{1 + \tfrac{1}{2}h_Y R_s\left(\dfrac{\partial\psi}{\partial\xi}\right)_0 + \tfrac{1}{8}h_Y^2 R_s^2\left(\dfrac{\partial\psi}{\partial\xi}\right)_0^2\right\}, & |\xi| \leqslant X_b, \end{cases}$$

$$c_3 = \begin{cases} E_0 h_Y^2 \left\{1 \pm \tfrac{1}{2}h_\xi \left[E_0 \pm R_s\left(\dfrac{\partial\psi}{\partial Y}\right)_0\right] + \tfrac{1}{8}h_\xi^2 \left[E_0 \pm R_s\left(\dfrac{\partial\psi}{\partial Y}\right)_0\right]^2\right\}, & |\xi| > X_b \\ h_Y^2 \left\{1 + \tfrac{1}{2}h_\xi R_s\left(\dfrac{\partial\psi}{\partial Y}\right)_0 + \tfrac{1}{8}h_\xi^2 R_s^2\left(\dfrac{\partial\psi}{\partial Y}\right)_0^2\right\}, & |\xi| \leqslant X_b, \end{cases}$$

$$c_4 = \begin{cases} h_\xi^2 \left\{1 - \tfrac{1}{2}h_Y R_s E_0\left(\dfrac{\partial\psi}{\partial\xi}\right)_0 + \tfrac{1}{8}h_Y^2 R_s^2 E_0^2\left(\dfrac{\partial\psi}{\partial\xi}\right)_0^2\right\}, & |\xi| > X_b \\ h_\xi^2 \left\{1 - \tfrac{1}{2}h_Y R_s\left(\dfrac{\partial\psi}{\partial\xi}\right)_0 + \tfrac{1}{8}h_Y^2 R_s^2\left(\dfrac{\partial\psi}{\partial\xi}\right)_0^2\right\}, & |\xi| \leqslant X_b, \end{cases}$$

$$c_0 = c_1 + c_2 + c_3 + c_4$$

and

$$b_1 = \begin{cases} h_Y^2 E_0^2 (1 \mp \tfrac{1}{2}h_\xi) \\ h_Y^2, \end{cases} \qquad b_3 = \begin{cases} h_Y^2 E_0^2 (1 \pm \tfrac{1}{2}h_\xi) \\ h_Y^2, \end{cases}$$

$$b_2 = b_4 = h_\xi^2, \quad b_0 = b_1 + b_2 + b_3 + b_4.$$

The matrices associated with the set of finite-difference equations (4.14) and (4.15) are diagonally dominant under all circumstances and therefore an over-relaxation iterative scheme may be employed in order to reduce the number of iterations required for convergence.

5. Numerical results

Calculations have been obtained for several values of the blockage ratio, $d/2\mathscr{L}$, from 0.25 to 0.75 which are $O(1)$, and they all show very similar trends. In order to be able to compare with the experimental data we have concentrated in this paper on

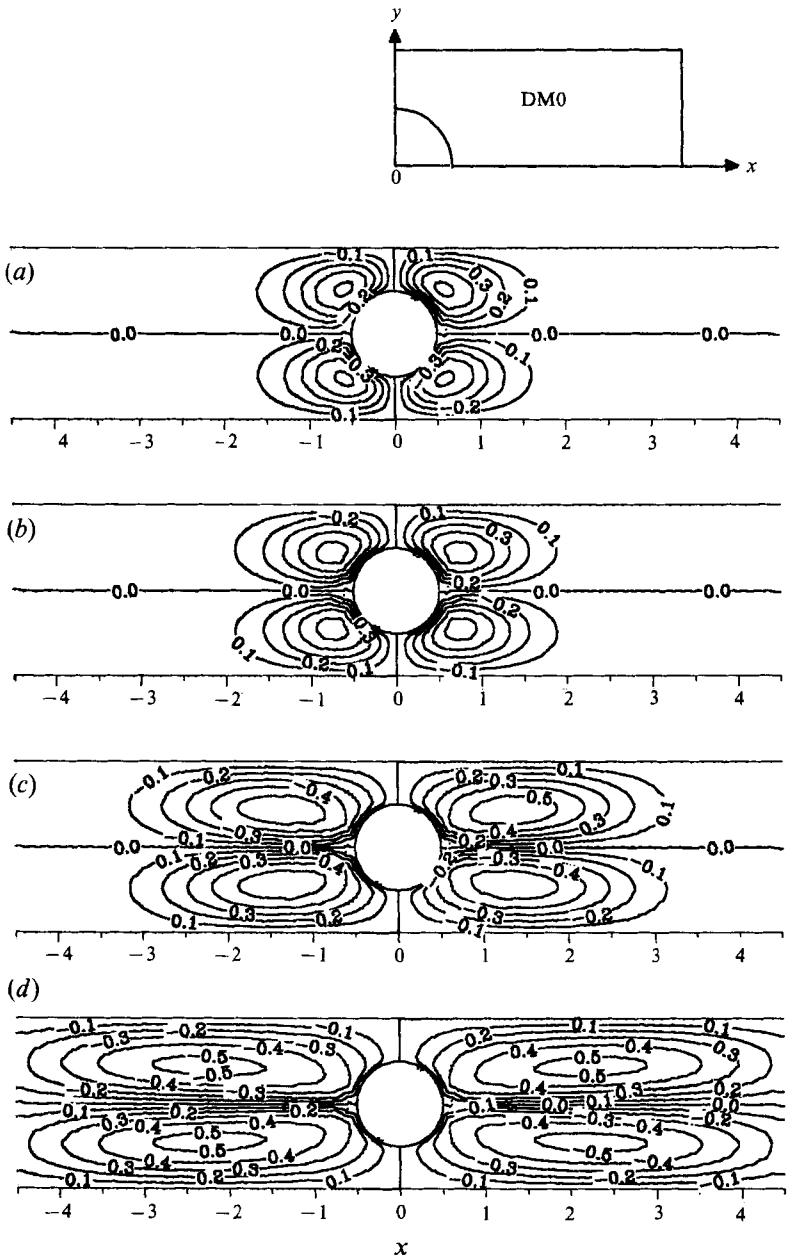

FIGURE 3. The streamlines for the outer streaming flow obtained by using DM0. (*a*) $R_s = 0.636$, (*b*) $R_s = 10$, (*c*) $R_s = 35$, (*d*) $R_s = 70$.

producing detailed results only for $L = 1$. It has been found that $x_R = 10$ is sufficiently large for $R_s \leqslant 15$, whilst $x_R = 15$ has to be used for $R_s > 15$ and $x_L = -x_R$ has been taken when a solution is required in $x < 0$. Mesh sizes $h_Y = 1/20$ and $h_\xi = X_b/25$ or $h_Y = 1/40$ and $h_\xi = X_b/50$ have been used depending on the value of the streaming Reynolds number. In order to reduce the complexity of the computer program it is convenient to take the mesh sizes on both sides of the lines $X = \pm X_b$ to have the same magnitude and hence the constant A_d in (4.7) is determined according to

$$h_\xi = \ln(1 + A_d h_\xi). \tag{5.1}$$

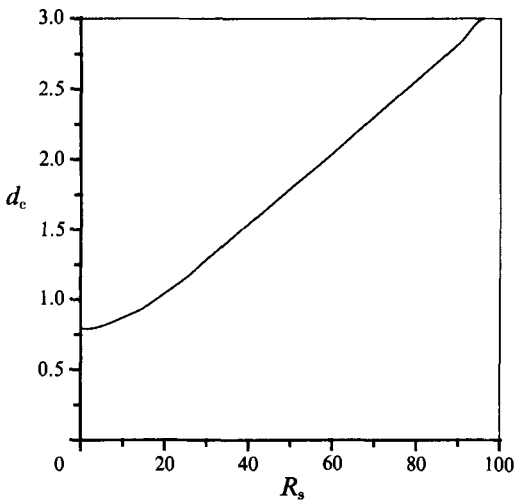

FIGURE 4. Distance between the centres of the recirculations and the axis of the nearest cylinder.

For $R_s \leqslant 15$ it is found that the results obtained with $h_\xi = X_b/25$ and $h_Y = 1/20$ are not significantly different from those obtained with $h_\xi = X_b/50$ and $h_Y = 1/40$. So the results shown here for $R_s \leqslant 15$ have been obtained with the larger mesh whilst the results for $R_s > 15$ have been obtained using the finer mesh. It has been found that further decreasing the mesh size for $R_s > 15$ results in solutions graphically indistinguishable from those obtained with $h_\xi = X_b/50$ and $h_Y = 1/40$.

5.1. *Boundary conditions DM0*

Numerical results have been obtained for values of R_s up to 100. Figure 3 shows the $O(\epsilon)$ outer steady streamlines for $R_s = 0.636$, 10, 35 and 70, using the solution domain and boundary condition described as DM0 in §4.1. The value of $R_s = 0.636$ was chosen as experimental results have been obtained for this value of the Reynolds number, see §6 (experimental data have also been obtained for $R_s = 2.54$ and 8.9). It is found from figure 3 that for $\epsilon \ll 1$ the $O(\epsilon)$ steady-state outer streamlines consist of four recirculating regions between each successive cylinder with the direction of the flow being along the direction of the oscillations away from each cylinder (i.e. along $y = 2kL$, where k is an integer) at a distance $O(1)$ from the body and towards $x = 0$ along $y = (2k+1)L$. The magnitudes of all the recirculations are very weak at large distances from the cascade and the general flow structure is very similar for all values of R_s. However, as the value of R_s increases then the centres of these four recirculating regions occur at increasing distances from the plane of the axes of the cylinders and the strengths of these circulations increase, see figures 3(*b*), 3(*c*) and 3(*d*). This is because more energy is being put into the system as the value of R_s increases. Figure 4 shows the variation of the minimum distance between the centre of each of the recirculating regions and the axis of the nearest cylinder, d_c, and the streaming Reynolds number, R_s. It is observed that, for $R_s \gtrsim 25$, d_c is almost directly proportional to R_s and we find that $d_c \approx 0.037R_s + 0.5$. Figure 5 shows the vorticity contours for the $O(\epsilon)$ steady outer streaming flow for $R_s = 0.636$, 10, 35 and 70, respectively, using the solution domain and boundary condition described as DM0. It is found that at $R_s = 0.636$ the vorticity along the surface of the cylinder is everywhere positive but, as the value of R_s increases, there develops a region near the cylinder of negative vorticity.

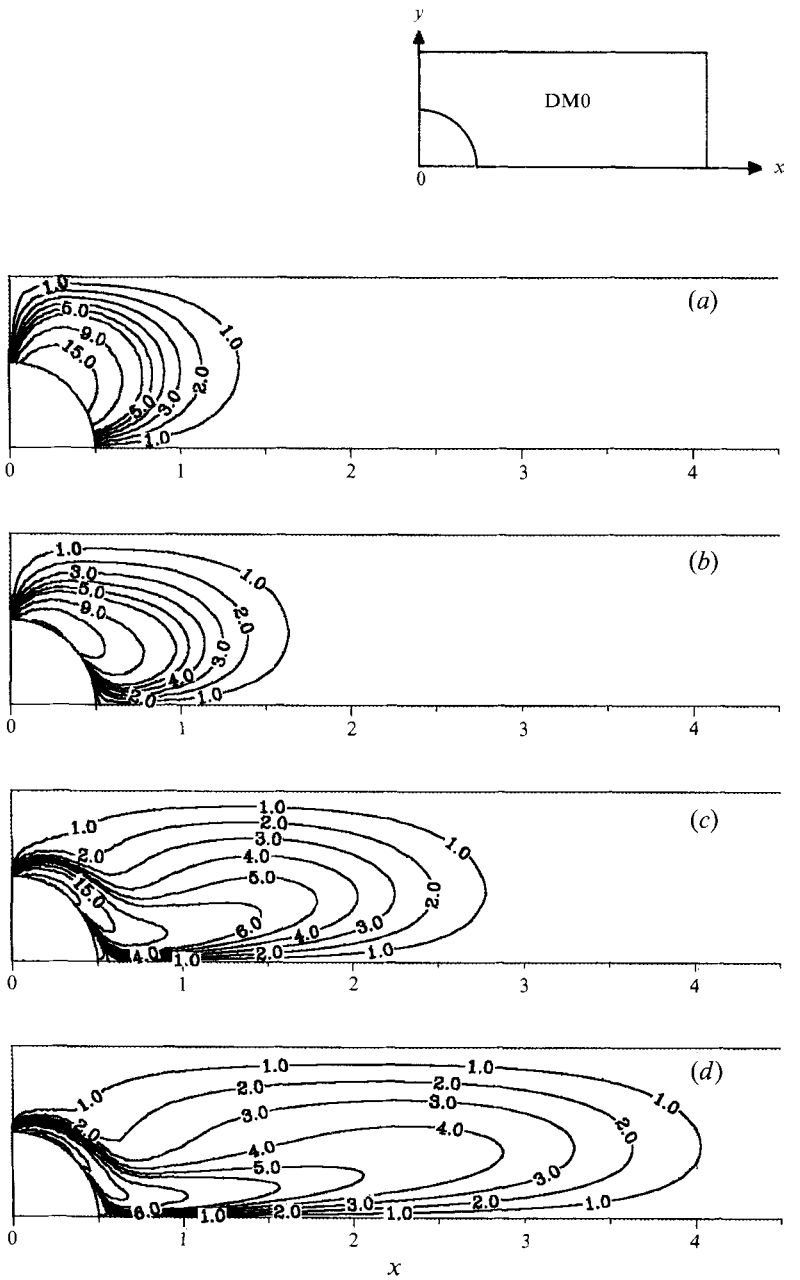

FIGURE 5. The vorticity contours for the outer streaming flow obtained by using DM0. (*a*) $R_s = 0.636$, (*b*) $R_s = 10$, (*c*) $R_s = 35$, (*d*) $R_s = 70$.

5.2. *Boundary conditions DM1*

Numerical results for the $O(\epsilon)$ outer steady streaming flow have been obtained for $R_s = 0.636, 2.54, 5, 6, 7, 8, 9, 10, 10.9, 15, 20, \ldots, 60$. Figure 6 shows the streamlines of the outer streaming flow with $R_s = 0.636$, 2.54 and 10.9 and it is clear that at the smaller values of R_s the streaming flow is almost symmetrical about both the axes $x = 0$ and $y = 0$, and the values of the streamfunctions on $y = L$ and $y = -L$ for any

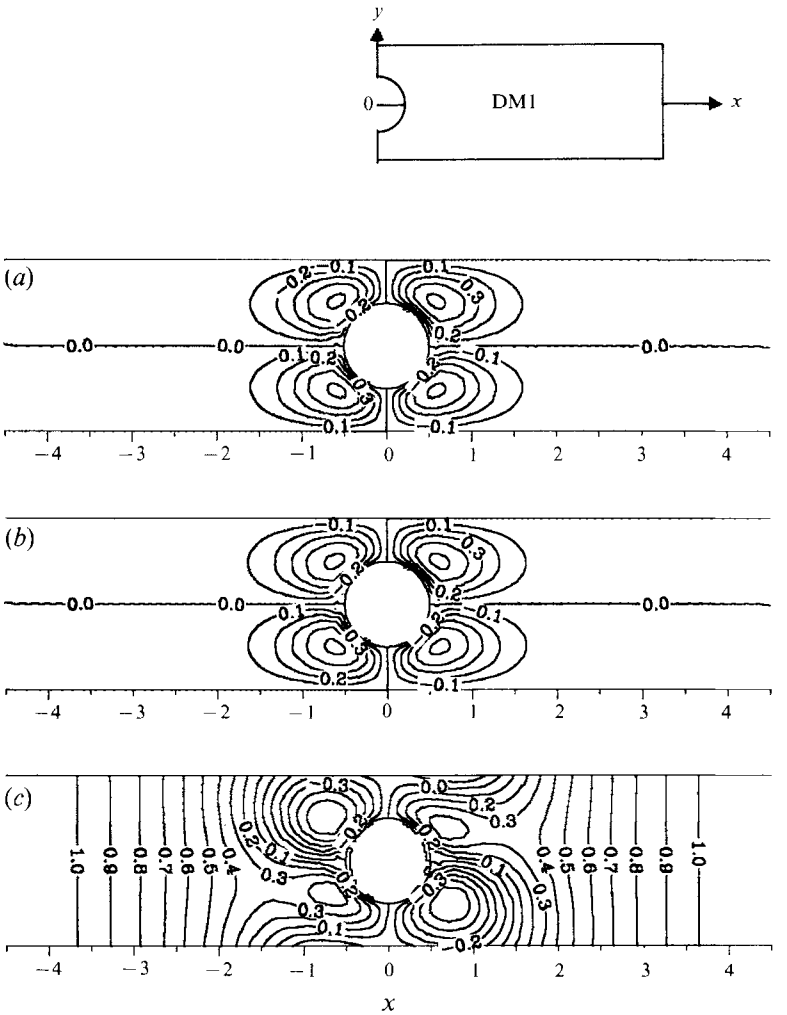

FIGURE 6. The streamlines for the outer streaming flow obtained by using DM1. (*a*) $R_s = 0.636$, (*b*) $R_s = 2.54$, (*c*) $R_s = 10.9$.

value of x are very small. Further, the results at the smaller values of R_s are almost identical to those obtained by using the boundary conditions described in DM0.

As the value of R_s increases, the symmetry of the numerical results begins to break down and the flow becomes asymmetrical. Instead of four recirculations of equal strength occurring between any two successive cylinders of the cascade, as there are at smaller values of R_s,. two of the recirculations become stronger than the other two (see figure 6). As a result fluid flows in the y-direction are generated at distances of just over one diameter from the cylinders, and the strength of this flow becomes stronger, at a given distance from the body, as the value of R_s increases but decreases in strength as $|x|$ increases.

The results indicate that there exists a critical value of R_s, R_{s0} say, such that $8 \lesssim R_{s0} \lesssim 9$ for which the flow is symmetrical about both the axes $x = 0$ and $y = 0$ for $R_s < R_{s0}$ and antisymmetrical for $R_s > R_{s0}$ (see figure 6). The induced velocity on $y = L$ in the y-direction for $R_s = 10$, 15, 20 and 25 as a function of x is shown in figure 7. It has been found that there exists a non-zero y-component of negative vertical

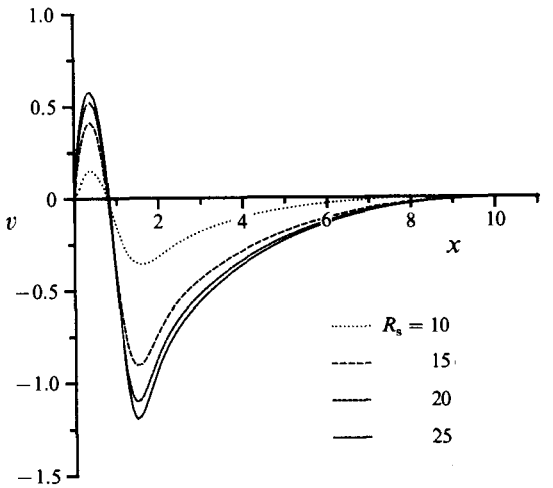

FIGURE 7. The vertical velocity at $y = 1$ as a function of x for $R_s = 15$.

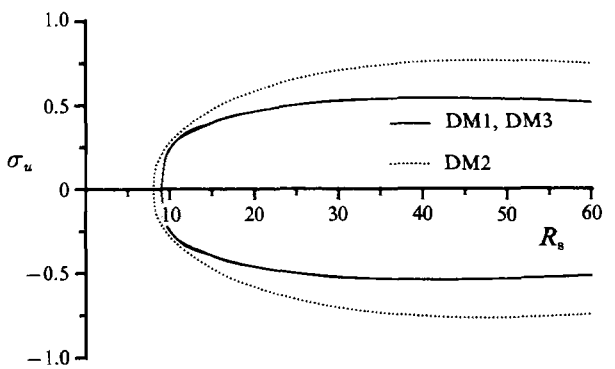

FIGURE 8. Bifurcation diagram of the streaming cascade flow (σ_u).

velocity for all values of R_s and this contrasts with the results obtained for $R_s < R_{s0}$ where the vertical velocity at $y = L$ is always zero.

In order to measure the asymmetry of the flow we define the quantities σ_u and σ_v such that

$$\sigma_u^2 = \int_{-L}^{L} |u|_{x=0}\,\mathrm{d}y \tag{5.2}$$

and

$$\sigma_v^2 = \int_{x_L}^{x_R} |v|_{y=L}\,\mathrm{d}x. \tag{5.3}$$

Physically, σ_u^2 represents the mass exchange across $x = 0$ in any interval $[2kL-L, 2kL+L]$ $(k = \pm 1, \pm 2, \ldots)$ and σ_v^2 the mass exchange across any line $y = (2k+1)L$ in the interval $[x_L, x_R]$. As x_L and x_R tend to $-\infty$ and $+\infty$, respectively, σ_v^2 becomes the total mass exchange across $y = (2k+1)L$.

The variations of σ_u and σ_v with R_s as obtained using the DM1 conditions are shown in figures 8 and 9, respectively. It is clear that both σ_u and σ_v are identically zero when $R_s \lesssim 8$ whilst they become non-zero when $R_s \gtrsim 9$, i.e. a bifurcation via the breakdown of symmetry occurs when the streaming Reynolds number lies somewhere between 8 and 9.

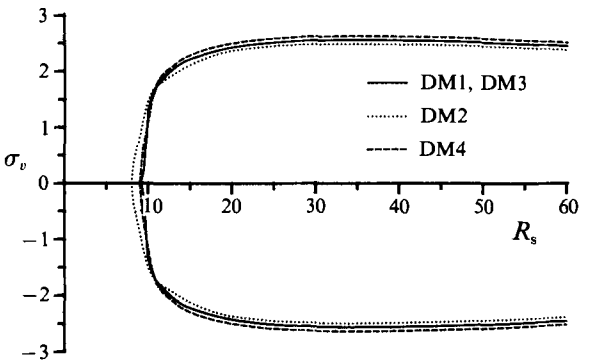

FIGURE 9. Bifurcation diagram of the streaming cascade flow (σ_v).

5.3. *Boundary conditions DM2*

Again, numerical results for the $O(\epsilon)$ outer steady streaming flow have been obtained for values of R_s between 0.636 and 60 as in §5.2. Figure 10 shows the streamlines for the outer streaming flow with $R_s = 0.636$, 2.54 and 10.9. It is again clear that the flow is almost symmetrical about the axes $x = 0$ and $y = 0$ at the smaller values of R_s but the flow becomes more asymmetrical as the value of R_s increases. The critical value for the streaming Reynolds number R_s was found to lie somewhere between 8 and 9 as was the case for the boundary conditions DM1.

Further the bifurcation diagrams of σ_u and σ_v for the different values of R_s that we have investigated are shown in figures 8 and 9, respectively. It is observed that the values of both σ_u and σ_v are almost zero when $R_s \lesssim 8$ whilst both of them are non-zero when $R_s \gtrsim 9$, i.e. the bifurcation via the breakdown of symmetry about both the x- and y-axes occurs at about the same value of R_s as they did for the boundary conditions DM1.

5.4. *Boundary conditions DM3*

Numerical results for the $O(\epsilon)$ outer streaming flow have been obtained for $R_s = 0.636$, $2.54, \ldots, 10.9, \ldots, 60$ and it is found that all of the results obtained are similar to those obtained when using DM1 and DM2. The critical value for R_s was, again, found to be between 8 and 9, and no further period-doubling solutions have been found for the values of R_s that we have investigated.

The values of quantities σ_u and σ_v as functions of R_s are plotted in figures 8 and 9 and it is observed the results show a very similar tendency to those obtained using DM1 and DM2. In particular, both σ_u and σ_v are almost identical to those obtained using the boundary conditions DM1. This is not surprising since the solutions here are periodic in the y-direction with a period of $2L$ and in this case the boundary conditions (4.3) are included in the boundary conditions (4.5); therefore the solutions obtained here should be identical to those obtained when using the boundary conditions DM1.

5.5. *Boundary conditions DM4*

Numerical results have been obtained for the $O(\epsilon)$ outer steady streaming flow for R_s between 0.636 and 60. It is found from these results that the streaming flow is symmetrical about both the axes $x = 0$ and $y = 0$ when $R_s \lesssim 8$ and this is consistent with the numerical results obtained when using the solution domains DM0, DM1, DM2 and DM3 subject to the corresponding boundary conditions. When $R_s \gtrsim 9$ the streaming flow is no longer symmetrical about the axis $y = 0$ and two of the four recirculation regions around each cylinder become stronger than the other two. In

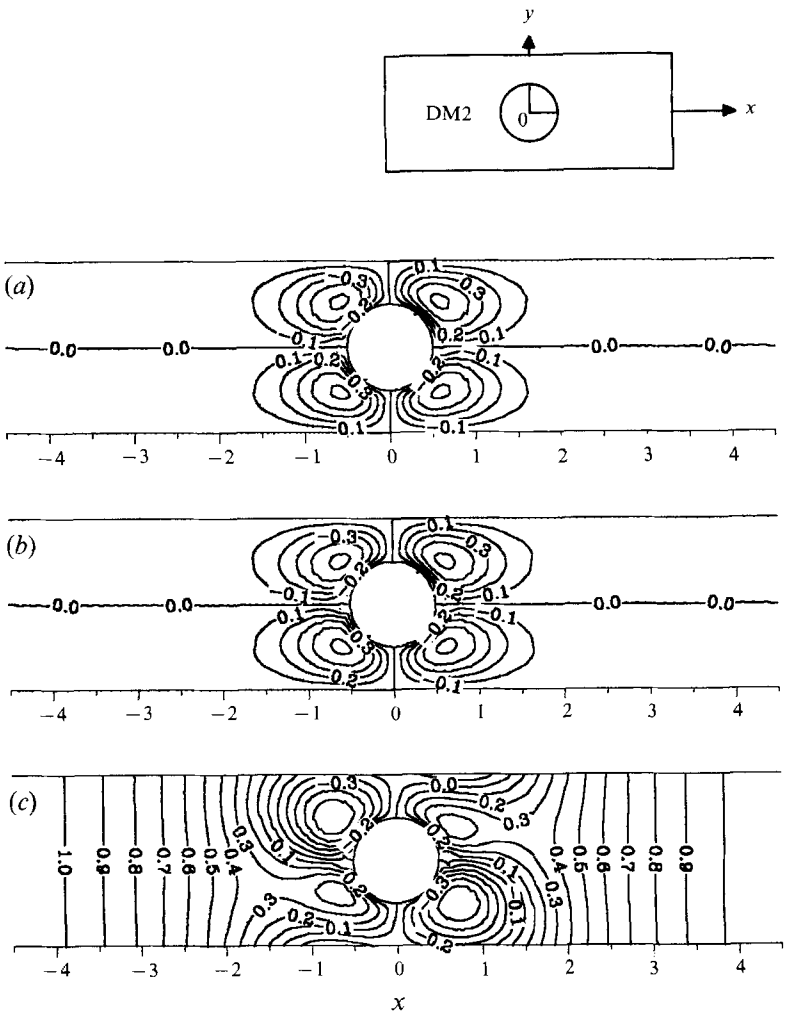

FIGURE 10. The streamlines for the outer streaming flow obtained by using DM2. (*a*) $R_s = 0.636$, (*b*) $R_s = 2.54$, (*c*) $R_s = 10.9$.

order to show the flow structure in this case the streamlines are plotted for $R_s = 8$, 15 and 25 in figure 11 where a clear tendency of how the flow structure changes with R_s can be observed.

The bifurcation diagrams for σ_u and σ_v as a function of R_s are plotted in figures 8 and 9. The values of σ_u are always zero as symmetrical boundary conditions have been used on $x = 0$, and clearly the tendency of σ_v is similar to those obtained when using the boundary conditions DM1, DM2 and DM3.

It is obvious from figures 8 and 9 that unless symmetry is enforced by the use of the boundary conditions DM0 then the streaming flow becomes asymmetrical either about $x = 0$ or $y = 0$ when $R_s \gtrsim 9$. This suggests that a bifurcation has occurred via the breakdown of symmetry. It is also noted from figure 8 that there is quite a big difference between the bifurcation curves using boundary conditions DM2 and those using the others and this suggests that there is a bigger mass exchange through $x = 0$ when using DM2 boundary conditions than when using the other boundary conditions.

Further, once a solution domain is taken which allows for the symmetry to be broken then the critical value of the streaming Reynolds number at which the solution

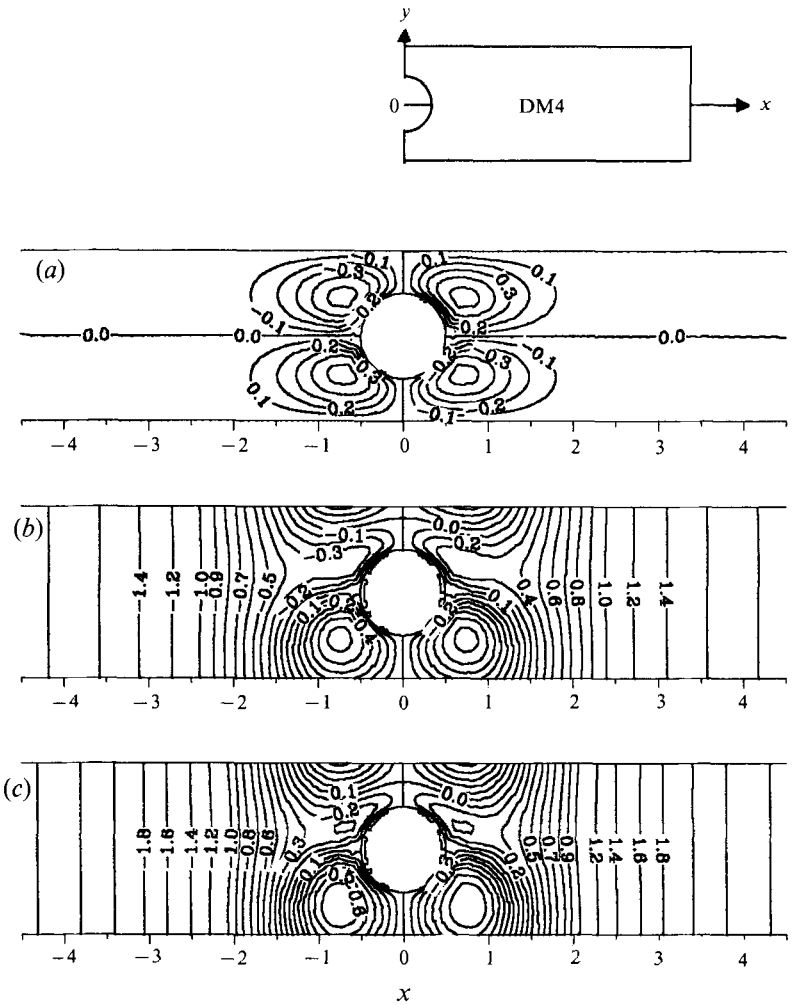

FIGURE 11. The streamlines for the outer streaming flow obtained by using DM4. (*a*) $R_s = 8$, (*b*) $R_s = 15$, (*c*) $R_s = 25$.

bifurcates is approximately the same for all the geometries considered in this paper. This may be why the breakdown to asymmetric flows is more complicated than that of the 'skew-symmetric' boundary condition DM1 and why it is impossible to postulate which set of boundary conditions may be deemed to be 'correct'.

6. Comparisons with experiments

6.1. *Flow visualization experiments*

A general schematic layout of the equipment in the Geophysical Fluid Dynamics Laboratory at Monash University that we used is shown in figure 12. The experiments were performed in a large rectangular tank of length 2 m and width 0.36 m, filled to a depth of approximately 0.20 m with water. Within this tank there was a smaller Perspex tank of length 1 m and width 0.14 m, filled with water to a depth of approximately 0.12 m. The smaller tank was fixed at about 0.04 m above the bottom of the larger tank. The temperature of the water in the outer tank was refrigerated and

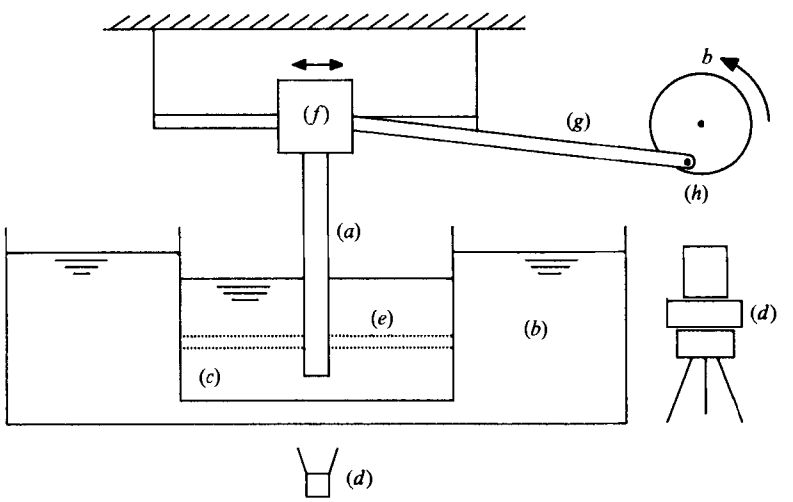

FIGURE 12. A schematic diagram of the experimental apparatus in the Geophysical Fluid Dynamics Laboratory at Monash University, Australia: (*a*) the cascade, (*b*) the refrigerated outer tank, (*c*) the inner tank, (*d*) the camera, (*e*) the illuminated strip of light, (*f*) a trolley which is free to move horizontally (the double arrows indicate the motion is harmonic), (*g*) the connecting rod and (*h*) a geared-down D.C. permanent magnet motor with a number of fixed displacement cams.

carefully controlled by having a large recirculation of water in the tank, so that the temperature on the boundary of the inner tank may be assumed constant. The water in the outer tank was slightly cooled so that there was no loss of heat from either the side or the bottom of the small tank. On top of the small tank a sheet of Perspex was placed, which was covered with bubble plastic in order for it float. The Perspex was painted black in order to reduce the reflection of the light and to increase the contrast in the photographs. However, the main aim of the covering of the top of the small tank was to reduce water evaporation from the surface, which causes recirculations. As we are investigating second-order effects it is absolutely essential that as much care as possible is taken in eliminating thermally driven flows even though they are very small. Throughout the experiments the temperature in the test tank was taken at numerous positions. It was found that typically the temperature in the test tank was position independent, being 12.2 °C$\pm$0.1 °C, whilst the ambient temperature was 19.6 °C and the dew point temperature 8.4 °C. The closeness of the temperatures of the small tank and the dew point ensures that only a very small amount of evaporation takes place. The surface temperature is higher than the sidewall temperature but this just ensures that the water is thermally stratified.

Harmonic oscillations were achieved by using a geared-down D.C. permanent magnet motor with a number of fixed displacement cams. From the cam a connecting rod is attached to a freely moving trolley which runs on top of the large tank. The cylinders were firmly fixed to the trolley such that they are vertical and at right angles to the axis of the small tank. The cascade was made from Perspex circular cylinders with uniform diameters 0.01 m, separated by uniform gaps of 0.01 m, i.e. $L = 1$. The cylinders were mounted such that the bottom of the tank and the teeth of the cascade were about 0.002 m above the bottom of the tank and extended out of the water. This configuration minimizes the end effects.

The visualization was achieved by seeding the entire water with polyester spheres used in Dulux emulsion paints. These spheres are coated with titanium oxide and have a mean diameter of 17 μm, with only 3% of the mass of particles having a diameter

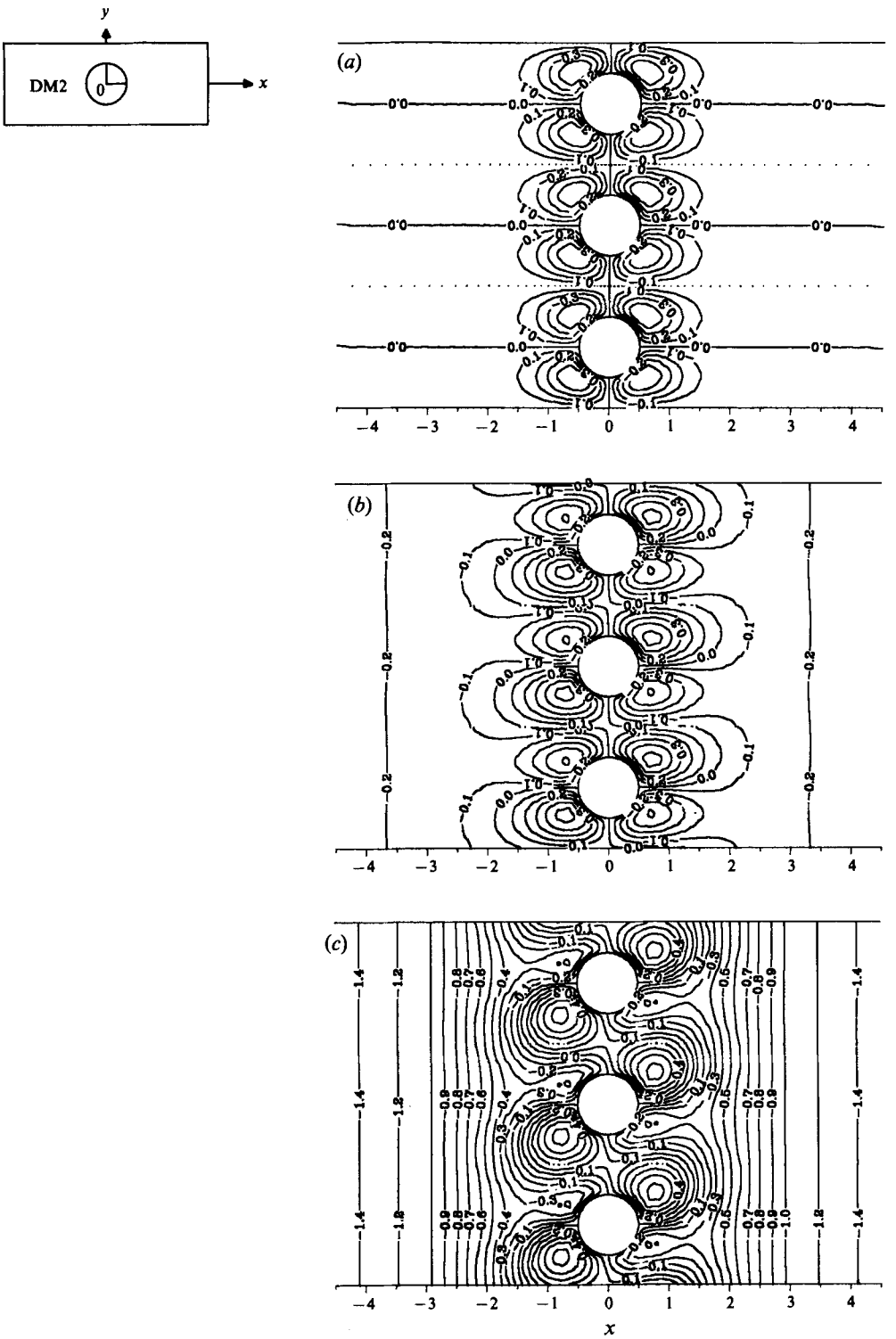

FIGURE 13. The streamlines from the numerical results for the outer streaming flow. (*a*) $R_s = 0.636$, (*b*) $R_s = 9$, (*c*) $R_s = 15$.

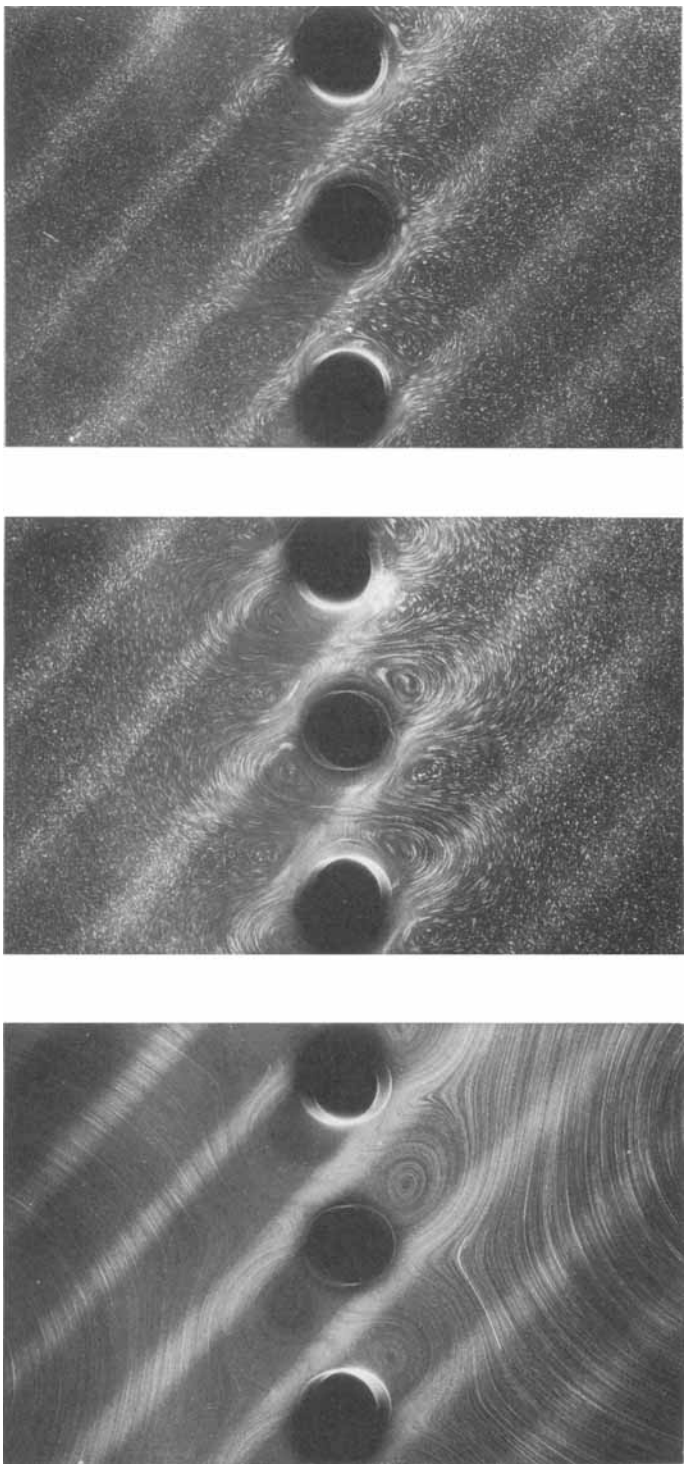

FIGURE 14. The experimental results for the outer streaming flow. (a) $R_s = 0.636$, (b) $R_s = 2.54$, (c) $R_s = 8.9$.

greater than 30 μm. The specific gravity varies but is generally within about 5% of that of water and hence the particles settle out of suspension extremely slowly. It is found they stay in suspension long enough for photographs to be taken over a period of about ten hours. However, the tank was stirred every four hours when performing the experiments. Further the length of time taken between photographing different runs varied according to the frequency and amplitude of the previous oscillation. It was found in all experiments performed here that if 20 minutes was left between each set of runs then the residual motion in the tank was minimal when viewing the flow.

The marker particles were illuminated using light from good quality projectors with slits in their focal planes focused into thin horizontal sheets of light between 0.002 and 0.005 m thickness in the working section. Two opposed projectors were required to obtain records adequately illuminated both upstream and downstream of the cascade from either side of the tank, with one projector upstream and one downstream at the moment of the record. The recording camera was fixed under the tanks and looked vertically down the face of the centre body of the cascade, and the thickness of the light sheet in the working section was chosen to illuminate just sufficient particles for a clear record in an exposure time which was about 10 times the period of oscillation of the cascade.

6.2. *Comparison of numerical results with experiments*

As we observed in §5 the numerical results obtained using the boundary conditions DM1, DM2, DM3 and DM4 are similar to each other for all the values of R_s that we have investigated. The numerical results for the steady streaming flow when $R_s = 0.636$, 9 and 15 are shown in figure 13 whilst the experimental results for $R_s = 0.636$, 2.54 and 8.9 are shown in figure 14 where the values of ϵ for the experimental data are 0.025, 0.05 and 0.05, respectively. Clearly the trend of the numerical results shows good agreement with the experimental investigations. It can be observed that the symmetry of the experimental result for $R_s = 0.636$ is good whilst for $R_s = 2.54$ the flow is starting to show signs of symmetry breaking. For $R_s = 8.9$ a breakdown in the symmetry is clearly observed from the experimental results and a comparison with the numerical results show qualitative agreement.

It should be noted that it is very hard to obtain exactly symmetrical experimental pictures even for very small values of R_s and it is extremely difficult to determine exactly the critical value of R_{s0} from the experimental work. The discrepancy between the experimental and numerical solutions is probably due to (i) the axes of the cylinders not being exactly in a plane; (ii) the use of a finite number of cylinders in the experimental work; (iii) the effects of the free surface and the bottom of the tank being at a finite distance from where the experimental results were obtained; and (iv) the value of ϵ being finite in the experiments.

It should be noted that on the photographs shown in figure 14 there is a diagonal pattern. This is caused by the use of light sources slanting rearwards to the left and forwards to the right; these produce bright diagonal bands where the marker particles are illuminated by both sources and darker bands of roughly half the intensity where one beam is obstructed by a tooth of the cascade.

7. Conclusions

The $O(\epsilon)$ outer steady streaming flow induced by a harmonically oscillating cascade of circular cylinders has been investigated both numerically and experimentally. The complex physical domain has been conformally transformed onto a rectangular solution domain and then the Navier–Stokes equations solved using a specialized

finite-difference technique. Various solution domains and boundary conditions have been applied in order to solve the problem and it is found that it is not always possible to obtain experimentally symmetrical flows for all values of the streaming Reynolds number R_s although, mathematically, symmetrical flows can always be predicted. The numerical results indicate that the boundary conditions on $y = kL$ (k an integer) are very important in predicting the observed flow. Numerical results for the flow field show a reasonable agreement with those obtained experimentally.

REFERENCES

BERTELSEN, A. F. 1974 An experimental investigation of high Reynolds number steady streaming generated by oscillating cylinders. *J. Fluid Mech.* **64**, 589–597.

BERTELSEN, A., SVARDAL, A. & TJOTTA, S. 1973 Nonlinear streaming effects associated with oscillating cylinders. *J. Fluid Mech.* **59**, 493–511.

DAVIDSON, B. J. & RILEY, N. 1972 Jet induced by oscillating motion. *J. Fluid Mech.* **53**, 287–303.

DENNIS, S. C. R. & HUDSON, J. D. 1978 A difference method for solving the Navier–Stokes equations. In *Proc. 1st Intl Conf. Numer. Methods in Laminar & Turbulent Flow*, pp. 69–80. Swansea: Pineridge.

FEARN, R. M., MULLIN, T. & CLIFFE, K. A. 1990 Nonlinear flow phenomena in a symmetric sudden expansion. *J. Fluid Mech.* **211**, 595–608.

HADDON, E. W. & RILEY, N. 1979 The steady streaming induced between oscillating circular cylinders. *Q. J. Mech. Appl. Maths* **32**, 265–282.

INGHAM, D. B., TANG, T. & MORTON, B. R. 1990 Steady two-dimensional flow through a row of normal flat plates. *J. Fluid Mech.* **210**, 281–302.

INGHAM, D. B. & YAN, B. 1989 The fluid flow induced by an oscillating cascade. In *Proc. 6th Conf. Numer. Methods in Laminar & Turbulent Flow*, pp. 723–733. Swansea: Pineridge.

INGHAM, D. B. & YAN, B. 1992 Fluid flow induced by a small amplitude harmonically oscillating cascade. *Acta Mechanica* **91**, 27–46.

INGHAM, D. B., YAN, B. & MORTON, B. R. 1992 The fluid flow induced by large amplitude oscillations of a cascade. *Computers Fluids* **21**, 305–321.

IRANI, M. B. 1982 Finite element analysis of viscous flow and rigid body interaction. Masters thesis, University of British Columbia.

KIM, S. K. & TROESCH, A. W. 1989 Streaming flows generated by high-frequency small-amplitude oscillations of arbitrarily shaped cylinders. *Phys. Fluids* A **1**, 975–985.

MANZOOR, M. 1984 *Heat Flow Through Extended Surface Heat Exchangers*. Lecture Notes in Engineering, vol. 5. Springer.

PATTANI, P. G. & OLSON, M. D. 1987 Rigid body-viscous interaction. *Intl J. Numer. Meth. Fluids* **7**, 653–695.

PATTANI, P. G. & OLSON, M. D. 1988 Force on oscillating bodies in viscous fluids. *Intl J. Numer. Meth. Fluids* **8**, 519–563.

RILEY, N. 1965 Oscillating viscous flows. *Mathematika* **12**, 161–175.

RILEY, N. 1967 Oscillatory viscous flows, review and extension. *J. Inst. Maths Applics.* **3**, 419–434.

SOBEY, I. J. & DRAZIN, P. G. 1986 Bifurcations of two-dimensional channel flows. *J. Fluid Mech.* **171**, 263–287.

STANSBY, P. K. & SMITH, P. A. 1991 Viscous forces on a circular cylinder in orbital flow at low Keulegan–Carpenter numbers. *J. Fluid Mech.* **229**, 159–171.

STUART, J. T. 1963 Unsteady boundary layers. In *Laminar Boundary Layers* (ed. L. Rosenhead), pp. 347–408. Oxford University Press.

STUART, J. T. 1966 Double boundary layers in oscillating viscous flows. *J. Fluid Mech.* **24**, 673–687.

TABAKOVA, S. & ZAPRYANOV, Z. 1982 On the hydrodynamic interaction of two spheres oscillating in a viscous fluid – I. Axisymmetrical case. *J. Appl. Maths. Phys.* **33**, 344–357.

TATSUNO, M. & BEARMAN, P. W. 1990 A visual study of the flow around an oscillatory circular cylinder at low Keulegan–Carpenter numbers and low Stokes numbers. *J. Fluid Mech.* **211**, 157–182.

THOMPSON, J. F., THAMES, F. C. & MASTIN, C. W. 1974 Automatic numerical grid generation of body fitted curvilinear coordinate systems for fields containing any number of arbitrary two dimensional bodies. *J. Comput. Phys.* **15**, 299–319.

WANG, C. Y. 1967 On high frequency oscillatory viscous flows. *J. Fluid Mech.* **32**, 55–68.

WILLIAMSON, C. H. K. 1985 Sinusoidal flow relative to circular cylinders. *J. Fluid Mech.* **155**, 141–174.

ZAPRYANOV, Z., KOZHOUKHAROVA, ZH. & IORDANOVA, A. 1988 On the hydrodynamic interaction of two circular cylinders oscillating in a viscous fluid. *Z. Angew. Maths. Phys.* **39**, 204–220.